

1 **Antarctic ice dynamics amplified by Northern Hemisphere sea-level forcing**

2

3 **Authors:** Natalya Gomez*¹, Michael E. Weber², Peter U. Clark^{3,4}, Jerry X. Mitrovica⁵,

4 Holly K. Han¹

5

6 1. Department of Earth and Planetary Sciences, McGill University, Montreal, QC, H3A
7 0E8, Canada

8 2. Department of Geochemistry and Petrology, Institute for Geosciences, University of
9 Bonn, Bonn, Germany

10 3. College of Earth, Ocean, and Atmospheric Sciences, Oregon State University, Corvallis,
11 OR, USA

12 4. School of Geography and Environmental Sciences, University of Ulster, Coleraine,
13 Northern Ireland, UK

14 5. Department of Earth and Planetary Sciences, Harvard University, Cambridge, MA, USA
15

16 **Abstract:**

17 A long-standing hypothesis for synchronous global ice-sheet evolution on orbital
18 timescales invokes an interhemispheric sea level forcing, whereby sea-level rise due to
19 ice loss in the Northern Hemisphere (NH) in response to insolation and greenhouse gas
20 forcing causes grounding line retreat of marine-based sectors of the Antarctic Ice Sheet
21 (AIS)¹⁻³. Recent evidence indicates that the AIS experienced substantial millennial-scale
22 variability during and after the last deglaciation⁴⁻⁷, further suggesting a possible sea-level
23 forcing. Global sea-level change from ice-sheet mass loss is strongly nonuniform⁸,
24 however, suggesting that the response of AIS grounding lines to NH sea-level forcing is
25 likely more complicated than previously considered^{1,2,6}. Here we show, using a coupled
26 ice sheet - global sea-level model, that a large or rapid NH sea-level forcing during

27 deglaciation reduces or exceeds the sea-level fall at AIS grounding lines driven by the
28 gravitational and deformational effects of AIS mass loss, enhancing grounding line
29 retreat and associated AIS mass loss. In contrast, during NH glaciation, the sea-level
30 forcing acts to enhance grounding-line advance. We find that including these effects
31 causes NH sea-level forcing to increase AIS volume during the Last Glacial Maximum
32 (LGM, ~26-20 ka) and triggers an earlier retreat and millennial scale variability through
33 the last deglaciation, consistent with geologic reconstructions of LGM AIS extent and
34 subsequent ice-sheet retreat and relative sea-level change in Antarctica^{3-7,9,10}.

35

36

37 **Main**

38 Several mechanisms exist to explain near-synchronous interhemispheric climate
39 changes on orbital timescales despite opposite insolation forcing^{11,12}. Synchronous
40 changes in surface climate, however, cannot explain synchronous changes in the
41 Northern Hemisphere (NH) and Antarctic ice sheets^{3,13} because they would have induced
42 opposing ice-sheet surface mass balance (SMB) responses, with warming climate over
43 the AIS leading to a more positive SMB³. In the absence of surface melting, mechanisms
44 that impact the primary controls on Antarctic Ice Sheet (AIS) mass balance (basal
45 melting of buttressing ice shelves and ice discharge across grounding lines of marine-
46 based sectors) are thus required for ice-sheet synchronization.

47 Studies have shown that an increase in subsurface warming from changes in ocean
48 circulation contributes to AIS deglaciation^{4,5,14,15}. Marine-based sectors of ice sheets are
49 also vulnerable to sea-level change at their grounding lines, whereby a local sea-level fall
50 may slow or stabilize grounding line retreat or initiate or enhance its advance, while a
51 sea-level rise may slow grounding line advance or initiate or enhance its retreat^{16,17}.

52 Previous work suggested that sea-level rise from deglaciation of NH ice sheets
53 triggered retreat of grounding lines of the AIS, thus synchronizing ice-sheet variability
54 globally^{1,2,18,19}. Well-dated geologic records of AIS fluctuations support synchronization
55 on orbital timescales^{3,13} and identify linkages between periods of sea-level rise and
56 millennial-scale AIS variability during the last deglaciation, 20 to 9 thousand years ago
57 (ka). For example, deep-sea sediments from Scotia Sea's Iceberg Alley record eight
58 discrete episodes of increased flux of iceberg-rafted debris (IBRD) originating from the
59 AIS during the last deglaciation⁴. Three of these AIS Discharge (AID) events occurred at

60 the same time as well-documented periods of sea-level rise, suggesting a possible
61 linkage: AID 7 corresponds to the onset of deglacial sea-level rise $\sim 19.5\text{-}19\text{ ka}^{3,20}$, AID 6
62 corresponds to Meltwater Pulse 1A (MWP-1A) $\sim 14.5\text{ ka}^{21}$, and AID 2 corresponds to an
63 acceleration of sea-level rise during the early Holocene starting at $\sim 11.5\text{ ka}^{22,23}$.
64 Additional evidence for this dynamic ice-sheet behavior comes from isotopic records
65 from a horizontal ice core in the Patriot Hills of the Weddell Sea Embayment⁶, which
66 suggest that the ice surface in that region lowered by $\geq 600\text{ m}$ during AID 6 and around
67 AID 2. Finally, marine records from the Ross Sea identify a step-wise retreat of the West
68 AIS grounding line coincident with AID 6 and AID 2 (ref. ⁷). The IBRD record suggests
69 that after AID 1 from $\sim 10.4\text{-}9\text{ ka}$, there was a substantial reduction in the amplitude of
70 iceberg-flux variability over the past 8 kyr^{24} , and global mean sea level (GMSL)
71 experienced only decimeter-scale changes over the last 6 kyr^{25} . Current uncertainties in
72 these far-field sea level reconstructions and the age model for Antarctic IBRD cores⁴
73 preclude a determination of the relative phasing between the AID events and the sea-level
74 change associated with NH ice melting, but modeling can provide insight into the
75 mechanisms that lead to these observed changes.

76 Here we investigate possible interhemispheric ice-sheet coupling through sea-level
77 change over the last 40 ky and assess its impact on AIS evolution and behavior. We
78 model the evolution of the AIS and global sea-level changes using the Pennsylvania State
79 University (PSU) 3-D ice-sheet model coupled to a gravitationally self-consistent global
80 sea-level model that includes viscoelastic deformation of the solid Earth, rotational
81 feedbacks, and migrating shorelines²⁶ (see Methods).

82

83 **Deglacial sea-level change in Antarctica**

84 Fig. 1a shows ice loss since 21 ka from the AIS as calculated in a coupled ice sheet
85 – sea level model simulation and from NH ice sheets derived from the ICE5G ice
86 history²⁷. The AIS simulation is based on parameters identified in a large ensemble
87 analysis as best-fitting a range of paleo and modern data constraints²⁸, and is
88 characterized by a GMSL equivalent mass loss of 5 m from the AIS, with 107 m from the
89 NH in ICE5G (see Methods and Extended Data Fig. 1 for results of simulations with a
90 larger AIS contribution to GMSL). Peak sea-level fall is predicted to reach 150 m in
91 previously glaciated regions in Antarctica while the bedrock deepens in the interior of
92 Antarctica and sea level rises by 150 m in the surrounding ocean (Fig. 1b). Mass loss
93 from NH ice sheets contributes a sea-level rise that increases from 80 m in East
94 Antarctica to 130 m in West Antarctica (Fig. 1c), in agreement with previous work³. This
95 sea-level gradient is driven by a shift of the Earth’s rotation axis towards North America
96 in the NH, where most ice is being lost (Fig. 1a), and towards East Antarctica in the
97 Southern Hemisphere, driving lower than average sea-level rise in these regions and
98 higher than average sea-level rise in the opposing quadrants of the Earth’s surface (which
99 include West Antarctica and Eurasia). In contrast, AIS mass loss drives a sea-level fall of
100 up to 300 m in previously glaciated regions of Antarctica due to gravitationally driven
101 lowering of the sea surface and viscoelastic uplift of the solid Earth under the areas of
102 mass loss (Fig. 1d). The sea-level fall associated with local AIS loss thus dominates the
103 total Antarctica signal in these areas, but sea-level rise from the much larger NH ice-mass
104 loss substantially decreases the geographic spread and magnitude of sea-level fall at
105 Antarctic grounding lines over the last deglaciation (compare Figs. 1b, d).

106 **AIS response to NH sea-level forcing**

107 To quantify how sea-level changes associated with NH ice-sheet variations (Figs.
108 1c, 2a) influenced AIS dynamics leading up to the Last Glacial Maximum (LGM, ~26-20
109 ka¹³) and during the last deglaciation, we compare AIS mass changes predicted from
110 model simulations that include the evolution of the NH ice sheets prescribed from five
111 ice-history reconstructions^{27,29-31} to those predicted from a simulation in which the NH
112 ice sheets remain fixed in their initial configuration at 40 ka and do not contribute to sea-
113 level changes in Antarctica over the simulation (Fig. 2b; Extended Data Figs 8;
114 Methods). In the simulations, NH ice growth leading up to the LGM contributes a sea-
115 level fall beginning at ~30 ka (Fig. 2a), which drives additional AIS growth at ~28 ka
116 (Fig. 2b). This growth occurs primarily in the Antarctic Peninsula and Weddell Sea
117 regions (Extended Data Figs. 2c and 3, at 20 ka; Extended Data Fig. 4) and is consistent
118 with evidence for when ice reached its LGM extent in these regions³.

119 During the last deglaciation, sea-level rise from NH ice-sheet retreat (Fig. 2a)
120 significantly enhances the magnitude and rate of AIS mass loss from 15 ka onward (Fig.
121 2b, Extended Data Figs. 2 and 3), whereas the simulation with no NH sea-level forcing is
122 characterized by net AIS growth over much of the same period (Fig. 2b). In particular,
123 with fixed NH ice, extensive grounded ice remains in the Weddell Sea and, to a lesser
124 extent, the Ross Sea regions until the present day (Extended Data Figs. 2 and 3), whereas
125 including a NH sea-level forcing causes these regions to completely deglacierate, reaching
126 a modern Antarctic ice volume close to the observed ($2.69 \times 10^7 \text{ km}^3$; ref. ³²). We note that
127 differences in AIS evolution are greatest in the Weddell Sea region (Extended Data Fig.
128 4) where the largest sea-level forcing is predicted from NH ice-mass loss (Fig. 1c). We

129 have highlighted the sensitivity of the ice sheet to this geographic variability in Extended
130 Data Fig. 7.

131

132 **MWP-1A and early Holocene ice loss**

133 Our simulations suggest that an increase in AIS mass loss after 15 ka driven by NH
134 sea-level forcing contributed to Meltwater Pulse 1A (MWP-1A) ~14.5 ka and support an
135 Antarctic source for early Holocene acceleration in sea-level rise (Bard et al., 2016) (Fig.
136 2). Specifically, the AIS simulations that include a NH sea-level forcing during the
137 deglaciation show distinct corresponding periods of rapid mass loss (Figs. 2b, 3a) during
138 and after the time of these two episodes of rapid sea-level rise. This behavior may thus
139 explain the large increases in IBRD flux in Iceberg Alley (AID events 6, 2 and 1, ref. 4;
140 Fig. 2c) and the evidence for mass loss from the Weddell Sea⁶ and Ross Sea⁷ regions at
141 these times. Alternate physical processes (such as ocean and atmospheric forcing) must
142 be sought to explain the remaining AID events during the last deglaciation⁴.

143 In the case of MWP-1A, the AIS experiences more extensive mass loss (Figs. 2b,
144 3a, and Extended Data Fig. 5) in the simulations in which NH ice sheets evolve relative
145 to the simulation where they are fixed and AIS mass loss is driven only by climate
146 forcing on the ice sheet¹⁴ (Figs. 3a-c). The net volume of ice lost in the latter simulation
147 over this period is 2.5–3 times less than predicted in the former across the range of
148 evolving NH ice histories we consider. In the case of the early Holocene, including NH
149 sea-level forcing increases the rate of AIS mass loss by up to a factor of ~4 starting at
150 ~11.5 ka (Fig. 3a), the time of MWP-1B suggested by the far-field Barbados sea-level
151 record²³ and AID 2 (ref. 4). This mass loss continues throughout AID 1 until between 9.5-

152 9 ka (Figs. 2, 3, Extended data Fig. 5), with substantial grounding line retreat in both the
153 Ross Sea and Weddell Sea regions (compare Figs. 3d and e). The amplified AIS response
154 during the early Holocene occurs regardless of whether there is an acceleration in NH ice
155 loss during that time or not (compare Extended Data Fig. 5a with ICE5G²⁷ and Figs. 5b-c
156 with ICE6G³¹ and ANU³⁰) and it is consistent with the hypothesis of a significant or
157 dominant Antarctic source for acceleration in GMSL rise^{31,33} during this period (see also
158 Extended Data Fig. 6).

159 We have confirmed that the general behavior evident in Figs. 2 and 3 holds for
160 coupled model simulations using a range of Earth and ice-model parameters (Extended
161 Data Figs. 1 and 8). The largest difference is found in simulations with less basal sliding.
162 These simulations result in a larger LGM ice sheet (Extended Data Fig. 1) with AIS
163 growth in the first half of the simulations being less sensitive to NH ice growth and the
164 associated sea-level fall than simulations with more basal sliding. The concordance
165 between the two simulations with less basal sliding is likely because the AIS margin
166 nearly reaches its maximum possible extent at the continental shelf edge in both cases.

167

168 **Comparison to geologic records**

169 We next consider local ice-sheet and sea-level changes in the Ross Sea region
170 where there are reconstructions of relative sea level^{9,34} (Southern Scott Coast, Site S in
171 Fig. 4a), grounding line migration⁷, and changes in ice-surface elevation (Site 1 in Fig. 4;
172 other sites in the Ross and Weddell Sea regions are discussed in Extended Data Figs. 10-
173 11)³⁵ that provide a test of the local response to NH sea-level forcing. When this forcing
174 is included, deglaciation of the region is predicted to begin in the early Holocene (Fig.

175 4a) with regional ice thinning occurring from 11 to 8 ka (blue, black and cyan curves
176 show thinning at both Sites S and 1 in Fig. 4b). This model result is consistent with
177 observations of ice-surface lowering at Site 1 (ref. ³⁵) (error bars, Fig. 4b; nearby Sites 3-
178 5 which are just outside of the region of substantial ice thinning, are discussed in
179 Extended Data Fig. 11), a major grounding line retreat of ≥ 200 km in the Ross Sea⁷ and a
180 peak IBRD flux during AID events 2 and 1 (ref. ⁴). In contrast, this retreat takes place
181 from 10 to 6 ka at Sites S and 1 when NH sea-level forcing is not included in the
182 simulation (Fig. 4b), which is also inconsistent with a relatively low observed IBRD flux
183 from ~ 8.5 ka onward²⁴ (grey line, Fig. 4b).

184 At Site S, local sea-level change during the deglacial phase is initially dominated
185 by NH-driven sea-level rise, but as local ice loss begins (~ 11 ka) the gravitational and
186 deformational effects associated with this ice loss dominate the local sea-level change
187 (Fig. 4c). When the NH-driven sea-level forcing is excluded (Fig. 4c), relative sea-level
188 fall is predicted to begin later, at ~ 9 ka, coincident with local ice loss for this simulation
189 shown in Fig. 4b, and there is almost no change in relative sea level prior to 10 ka. The
190 oldest relative sea-level indicators from this area (~ 6.5 ka; Fig. 4c) are more consistent
191 with the lower relative sea level predicted by the simulations that include the NH sea-
192 level forcing, but older indicators are needed to clearly corroborate this, especially given
193 the uncertainty in local viscoelastic Earth structure.

194

195 **Summary**

196 We conclude that geographically variable sea-level changes around Antarctica
197 driven by NH ice-sheet changes strongly modulated AIS growth and decay. In particular,

198 NH ice growth leading up to the LGM causes local sea-level fall and further AIS growth
199 in our simulations, yielding a higher peak AIS volume at the LGM than without this
200 forcing. Conversely, NH ice loss during the last deglaciation produces a sea-level rise of
201 80–130 m in Antarctica in our model, driving earlier, greater and more rapid AIS retreat
202 that is in better agreement with geological evidence than predictions that omit this
203 forcing. The simulations indicate that the Weddell Sea region of the AIS was subject to
204 the largest sea-level changes driven by NH ice changes, suggesting that ice-mass changes
205 in this region were particularly sensitive to this far-field sea-level forcing. Finally,
206 simulations with NH sea-level forcing predict increases in AIS mass flux during MWP-
207 1A and the early Holocene, consistent with multiple lines of geologic evidence for AIS
208 mass loss at these times.

209

210 **References:**

211

- 212 1 Denton, G. H. & Hughes, T. J. Milankovitch theory of ice ages: Hypothesis of
213 ice-sheet linkage between regional insolation and global climate. *Quaternary*
214 *Research* **20**, 125-144 (1983).
- 215 2 Huybrechts, P. J. Sea-level changes at the LGM from ice-dynamic
216 reconstructions of the Greenland and Antarctic ice sheets during the glacial
217 cycles. *Quaternary Science Reviews* **21**, 203-231 (2002).
- 218 3 Weber, M. E. *et al.* Interhemispheric ice-sheet synchronicity during the Last
219 Glacial Maximum. *Science* **334**, 1265-1269, doi:10.1126/science.1209299
220 (2011).
- 221 4 Weber, M. E. *et al.* Millennial-scale variability in Antarctic ice-sheet discharge
222 during the last deglaciation. *Nature* **510**, 134-138, doi:10.1038/nature13397
223 (2014).
- 224 5 Golledge, N. R. *et al.* Antarctic contribution to meltwater pulse 1A from
225 reduced Southern Ocean overturning. *Nature Communications* **5**, 5107,
226 doi:10.1038/ncomms6107 (2014).
- 227 6 Fogwill, C. J. *et al.* Antarctic ice sheet discharge driven by atmosphere-ocean
228 feedbacks at the Last Glacial Termination. *Scientific Reports* **7**, 39979,
229 doi:10.1038/srep39979 (2017).
- 230 7 Bart, P. J., DeCesare, M., Rosenheim, B. E., Majewski, W. & McGlannan, A. A
231 centuries-long delay between a paleo-ice-shelf collapse and grounding-line

232 retreat in the Whales Deep Basin, eastern Ross Sea, Antarctica. *Scientific*
233 *Reports* **8**, 12392, doi:10.1038/s41598-018-29911-8 (2018).

234 8 Milne, G. A. & Mitrovica, J. X. Searching for eustasy in deglacial sea-level
235 histories. *Quaternary Science Reviews* **27**, 2292-2302,
236 doi:10.1016/j.quascirev.2008.08.018 (2008).

237 9 Hall, B. L. & Denton, G. H. New relative sea - level curves for the southern
238 Scott Coast, Antarctica: evidence for Holocene deglaciation of the western
239 Ross Sea. *Journal of Quaternary Science* **14**, 641-650 (1999).

240 10 Fogwill, C. J. *et al.* Southern Ocean carbon sink enhanced by sea-ice feedbacks
241 at the Antarctic Cold Reversal. *Nature Geoscience*, doi:10.1038/s41561-020-
242 0587-0 (2020).

243 11 Kawamura, K. *et al.* Northern Hemisphere forcing of climatic cycles in
244 Antarctica over the past 360,000 years. *Nature* **448**, 912-916 (2007).

245 12 Huybers, P. & Denton, G. Antarctic temperature at orbital timescales
246 controlled by local summer duration. *Nature Geoscience* **1**, 787-792 (2008).

247 13 Clark, P. U. *et al.* The last glacial maximum. *Science* **325**, 710-714 (2009).

248 14 Pollard, D., Chang, W., Haran, M., Applegate, P. & DeConto, R. Large ensemble
249 modeling of the last deglacial retreat of the West Antarctic Ice Sheet:
250 comparison of simple and advanced statistical techniques. *Geoscientific Model*
251 *Development* **9**, 1697-1723, doi:10.5194/gmd-9-1697-2016 (2016).

252 15 Clark, P. U. *et al.* Oceanic forcing of penultimate deglacial and last interglacial
253 sea-level rise. *Nature* **577**, 660-664 (2020).

254 16 Weertman, J. Stability of the junction of an ice sheet and an ice shelf. *Journal*
255 *of Glaciology* **13**, 3, doi:10.1017/s0022143000023327 (1974).

256 17 Schoof, C. Ice sheet grounding line dynamics: Steady states, stability, and
257 hysteresis. *Journal of Geophysical Research* **112**, F03S28-19,
258 doi:10.1029/2006JF000664 (2007).

259 18 Denton, G. H., Hughes, T. J. & Karlén, W. Global ice-sheet system interlocked
260 by sea level. *Quaternary Research* **26**, 3-26 (1986).

261 19 Tigchelaar, M., Timmermann, A., Friedrich, T., Heinemann, M. & Pollard, D.
262 Nonlinear response of the Antarctic Ice Sheet to late Quaternary sea level and
263 climate forcing. *Cryosphere* **13** (2019).

264 20 Yokoyama, Y., Lambeck, K., De Deckker, P., Johnston, P. & Fifield, L. K. Timing
265 of the Last Glacial Maximum from observed sea-level minima. *Nature* **406**,
266 713-716, doi:10.1038/35021035 (2000).

267 21 Deschamps, P. *et al.* Ice-sheet collapse and sea-level rise at the Bølling
268 warming 14,600 years ago. *Nature* **483**, 559-564, doi:10.1038/nature10902
269 (2012).

270 22 Bard, E., Hamelin, B. & Delanghe-Sabatier, D. Deglacial Meltwater Pulse 1B
271 and Younger Dryas sea levels revisited with boreholes at Tahiti. *Science* **327**,
272 1235-1237, doi:10.1126/science.1180557 (2010).

273 23 Abdul, N. A., Mortlock, R. A., Wright, J. D. & Fairbanks, R. G. Younger Dryas sea
274 level and meltwater pulse 1B recorded in Barbados reef crest coral *Acropora*
275 *palmata*. *Paleoceanography* **31**, 330-344, doi:10.1002/2015PA002847
276 (2016).

- 277 24 Bakker, P., Clark, P. U., Golledge, N. R., Schmittner, A. & Weber, M. E.
 278 Centennial-scale Holocene climate variations amplified by Antarctic Ice Sheet
 279 discharge. *Nature* **541**, 72-76, doi:10.1038/nature20582 (2017).
- 280 25 Hallmann, N. *et al.* Ice volume and climate changes from a 6000 year sea-level
 281 record in French Polynesia. *Nature Communications* **9**, 285,
 282 doi:10.1038/s41467-017-02695-7 (2018).
- 283 26 Gomez, N., Pollard, D. & Mitrovica, J. X. A 3-D coupled ice sheet – sea level
 284 model applied to Antarctica through the last 40 ky. *Earth and Planetary
 285 Science Letters* **384**, 88-99 (2013).
- 286 27 Peltier, W. R. Global glacial isostasy and the surface of the ice-age Earth: the
 287 ICE-5G (VM2) model and GRACE. *Annual Review of Earth and Planetary
 288 Sciences* **32**, 111, doi:10.1146/annurev.earth.32.082503.144359 (2004).
- 289 28 Pollard, D., Gomez, N. & DeConto, R. M. Variations of the Antarctic Ice Sheet in
 290 a coupled ice sheet-Earth-sea level model: Sensitivity to viscoelastic Earth
 291 properties. *Journal of Geophysical Research: Earth Surface* **122**, 2124-2138,
 292 doi:10.1002/2017JF004371 (2017).
- 293 29 Tarasov, L., Dyke, A. S., Neal, R. M. & Peltier, W. R. A data-calibrated
 294 distribution of deglacial chronologies for the North American ice complex
 295 from glaciological modeling. *Earth and Planetary Science Letters* **315**, 30-40
 296 (2012).
- 297 30 Lambeck, K., Rouby, H. & Purcell, A. Sea level and global ice volumes from the
 298 Last Glacial Maximum to the Holocene. *Proceedings of the National Academy
 299 of Sciences* **111**, 15296, doi:10.1073/pnas.1411762111 (2014).
- 300 31 Peltier, W. R., Argus, D. F. & Drummond, R. Space geodesy constrains ice age
 301 terminal deglaciation: The global ICE-6G_C (VM5a) model. *Journal of
 302 Geophysical Research: Solid Earth* **120**, 450-487 (2015).
- 303 32 Fretwell, P. *et al.* Bedmap2: Improved ice bed, surface and thickness datasets
 304 for Antarctica. *The Cryosphere* **7.1**, 375-393 (2013).
- 305 33 Bard, E., Hamelin, B., Deschamps, P. & Camoin, G. Comment on “Younger
 306 Dryas sea level and meltwater pulse 1B recorded in Barbados reefal crest
 307 coral *Acropora palmata*” by N. A. Abdul *et al.* *Paleoceanography* **31**, 1603-
 308 1608, doi:10.1002/2016PA002979 (2016).
- 309 34 Briggs, R. D. & Tarasov, L. How to evaluate model-derived deglaciation
 310 chronologies: a case study using Antarctica. *Quaternary Science Reviews* **63**,
 311 109-127, doi:10.1016/j.quascirev.2012.11.021 (2013).
- 312 35 Jones, R., Whitehouse, P., Bentley, M., Small, D. & Dalton, A. Impact of glacial
 313 isostatic adjustment on cosmogenic surface-exposure dating. *Quaternary
 314 Science Reviews* **212**, 206-212 (2019).

315
 316

317 **Main Text Figure Captions:**

318

319 **Figure 1: Contributions to deglacial sea-level changes in Antarctica.** (a) Grounded
 320 ice-thickness changes in meters since 21 ka in the coupled ice sheet – sea level
 321 simulation, based on the ICE5G²⁷ ice history in the NH and the dynamic ice-sheet model

322 in Antarctica. (b) Predicted total relative sea-level change, in meters, since 21 ka in
323 Antarctica. (c) Component of frame (b) associated with ice-cover changes in the NH in
324 the ICE5G²⁷ ice history, computed from a simulation with the sea-level model alone. (d)
325 Difference between frames (b) and (c), showing changes in relative sea level associated
326 with Antarctic ice-cover changes.

327

328 **Figure 2: Timing of NH sea level forcing and its influence on Antarctic ice volume**
329 **changes.** (a) Prescribed changes in NH ice volume from the ICE5G²⁷ (solid black line),
330 ICE6GC³¹ (dashed black line) and the ANU³⁰ (cyan) ice histories, as well as two
331 composite ice histories in which ice cover over North America and Greenland in ICE5G
332 has been replaced by GLAC1D²⁹ regional ice histories (blue lines). Blue vertical bands
333 indicate the timing of MWP-1A²¹ and MWP-1B²². (b) Changes in Antarctic ice volume
334 predicted in simulations with fixed (red line) and evolving NH ice taken from the ice
335 histories shown in frame (a) (blue, cyan and black lines). Green vertical bands indicate
336 periods during MWP-1A and the earth Holocene in the model simulations that are
337 examined in the text and other figures. (c) Iceberg rafted debris flux from sediment cores
338 in Iceberg Alley⁴ adopting the AIC 2012 model (see Methods and Extended Data Figure
339 9). Vertical red bands indicate the timing of AIS Discharge (AID) events, 1, 2 and 6 as
340 labeled, and horizontal blue bands indicate the timing of Last Glacial Maximum extent in
341 Weddell Sea (LGM WS)³.

342

343 **Figure 3: Enhanced Antarctic ice loss during MWP-1A and the early Holocene.** (a)
344 Rate of change of Antarctic ice volume, including grounded and floating ice, calculated
345 as a 100-year running mean, predicted from simulations including (black line) and
346 excluding (red line) NH ice-cover changes. The black line and shading represent the
347 mean and standard deviation of predictions generated with the five ice histories described
348 in the text. (b–e) Change in Antarctic ice thickness during (b,c) MWP-1A from 14.5–13.5
349 ka, and (d,e) the early Holocene starting from the time of MWP-1B from 11.5-9 ka.
350 Frames (b,d) are based on simulations which include ice mass flux from the NH from the
351 ICE5G ice history. These simulations predict Antarctica ice loss equivalent to a GMSL
352 rise of 1.14 m and 1.95 m across the MWP-1A and early Holocene time windows,
353 respectively. Frames (c,e) are generated from simulations in which NH ice sheets remain
354 fixed throughout the simulation. Grey-blue and black lines in (b–e) indicate the
355 grounding line position at the start and end of the time interval, respectively.

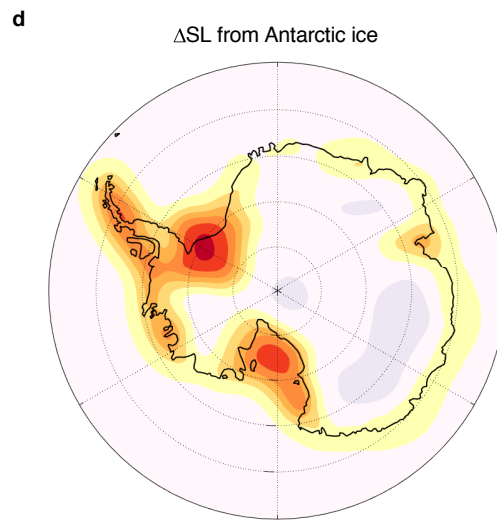
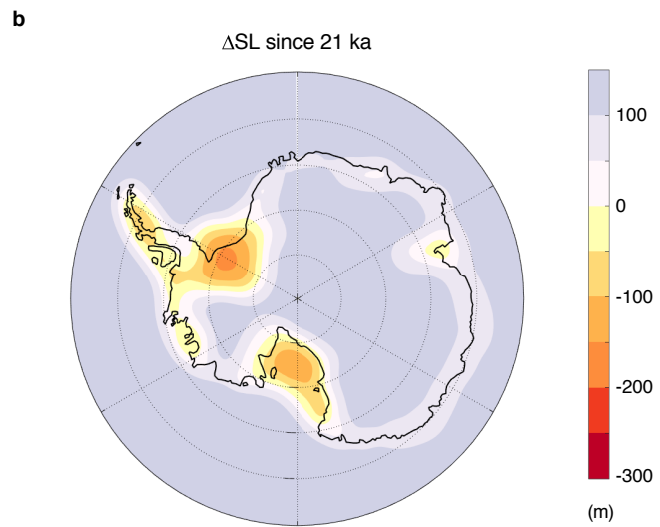
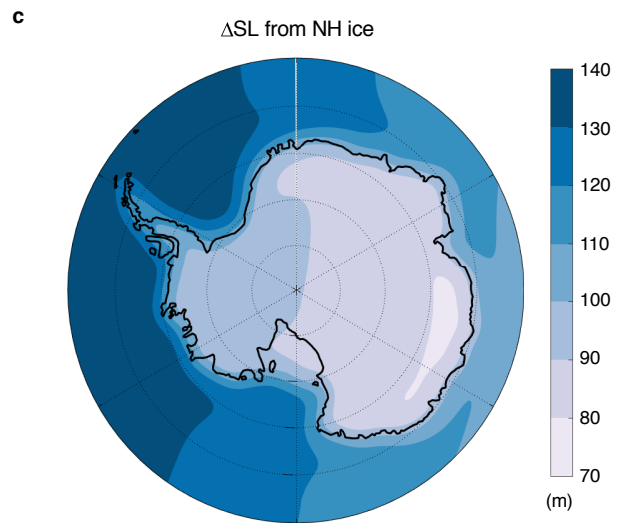
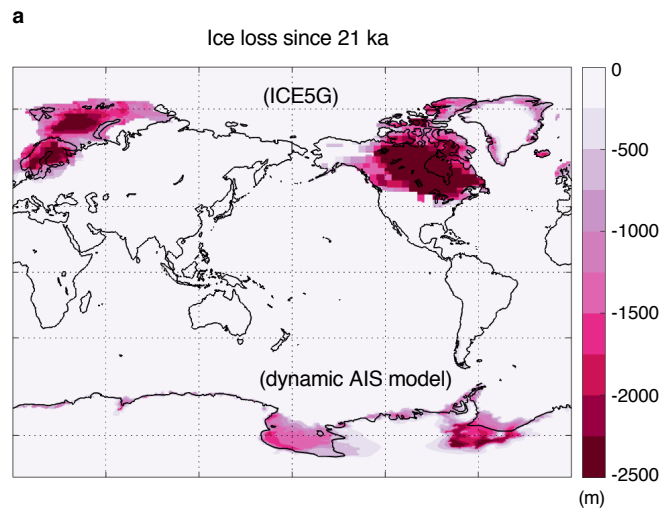
356

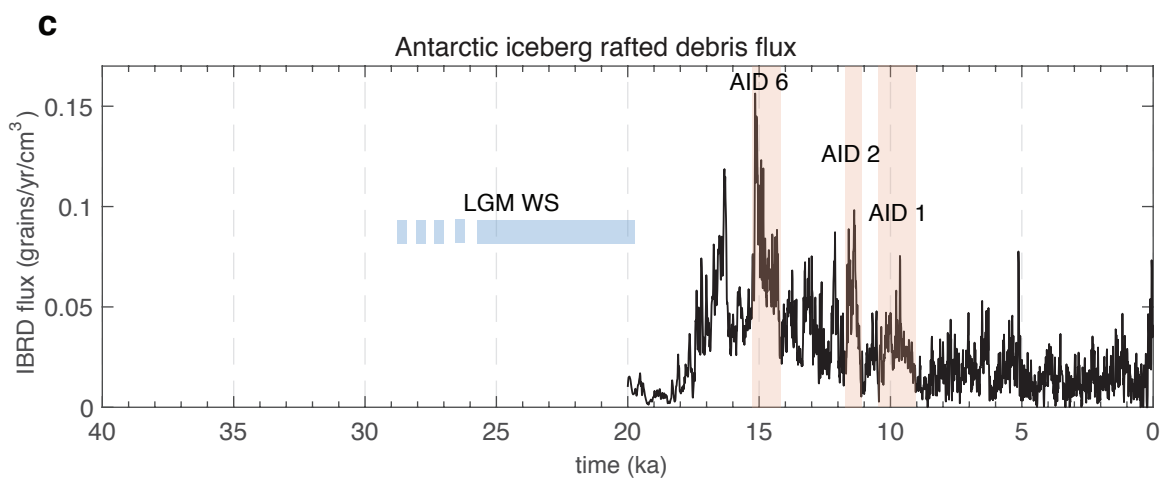
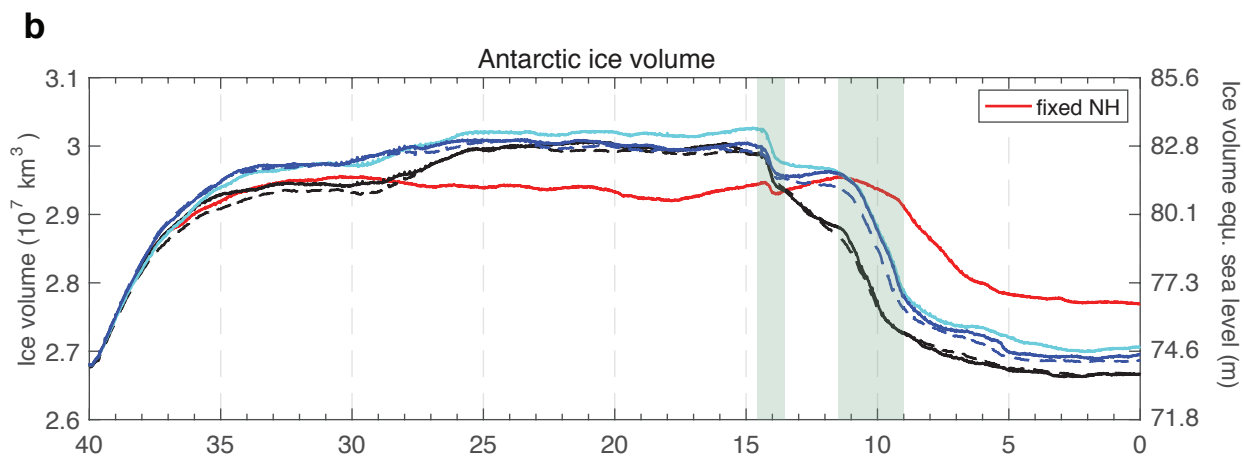
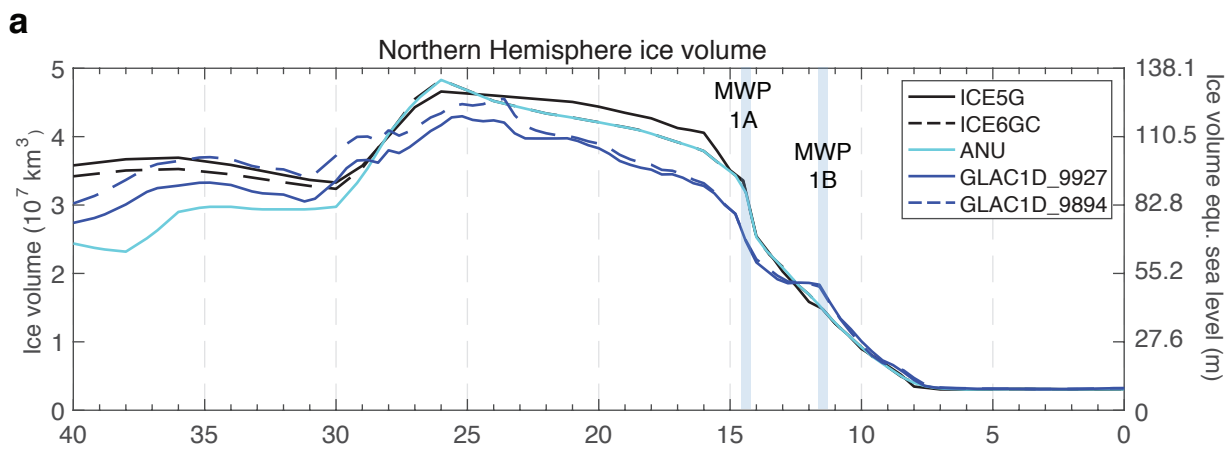
357 **Figure 4: Agreement of predicted sea-level and ice-cover changes with geological**
358 **records in the Ross Sea sector.** (a) Predicted Antarctic ice cover in the simulation that
359 includes NH ice from ICE5G²⁷ at snapshots in time as the Ross Sea region deglaciates.
360 (b) Predicted ice-thickness above modern thickness in meters at Site S, indicated by the
361 red dots in (a), and Site 1 from ref. ³⁵, indicated by the blue dots in (a), for simulations in
362 which NH ice cover is evolving according to ICE5G²⁷ and ANU³⁰ ice histories (black and
363 cyan lines for Site S, solid blue line for Site 1) and fixed (red line for Site S, dashed blue
364 line for Site 1). Error bars show cosmogenic exposure age data with 2σ uncertainty from
365 ref. ³⁵ at Site 1. The grey time series is the recorded flux of Antarctic iceberg-rafted
366 debris (IBRD) in grains/yr/cm³ shown in Fig. 2c, and red vertical bands indicate AIDs 1
367 and 2. (c) Predictions of relative sea-level change at Site S for the cases of evolving

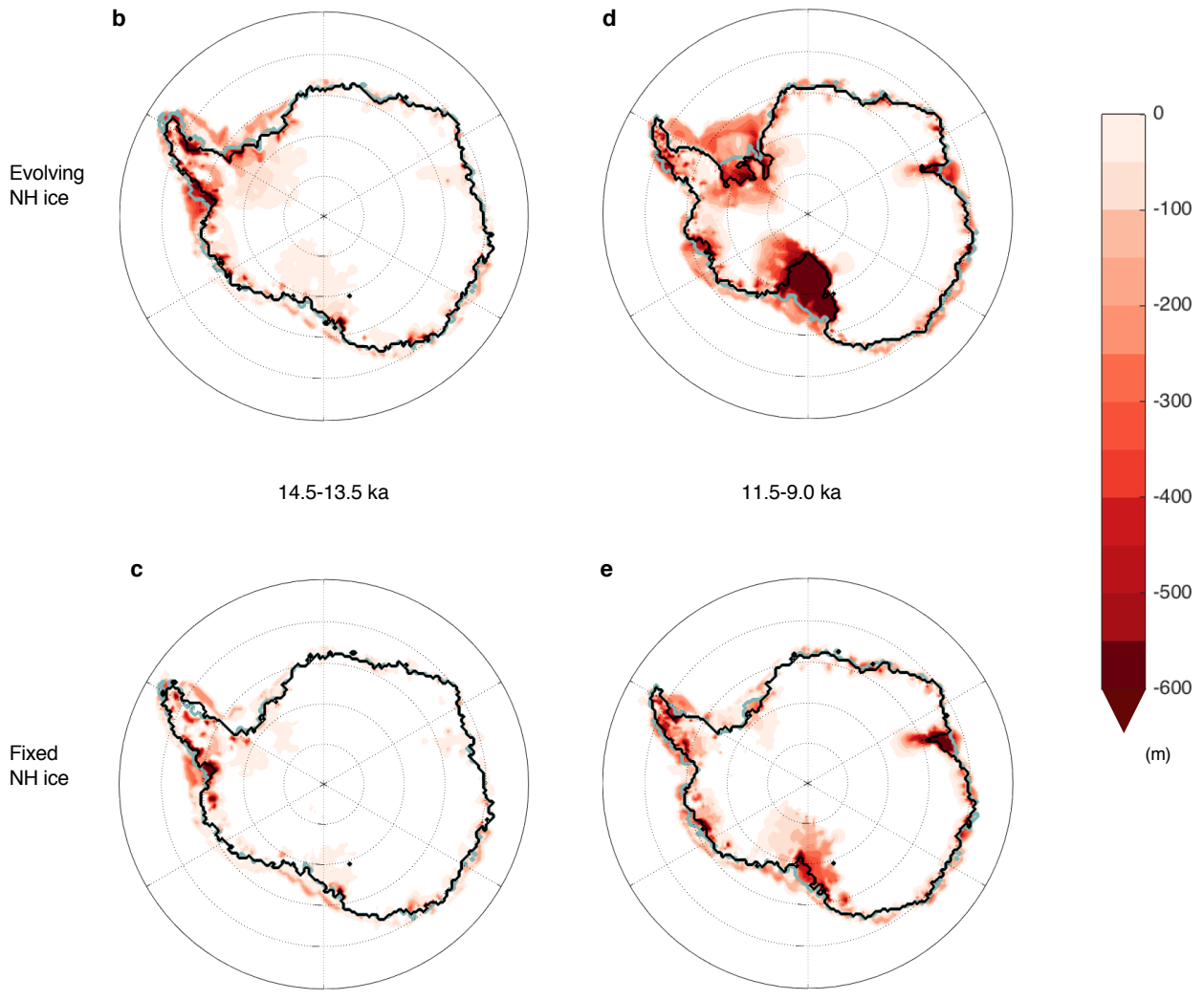
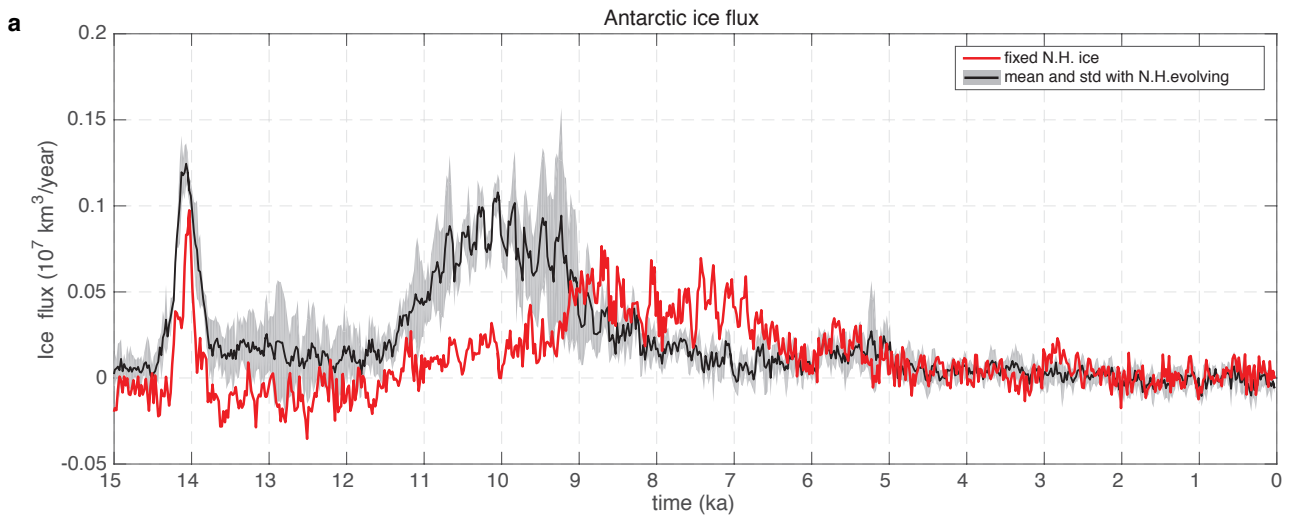
368 (black and cyan lines) and fixed (red line) NH ice cover. Dashed black and cyan lines in
369 (c) indicate the contribution to GMSL change from NH ice-cover prescribed in the
370 ICE5G²⁷ (solid blue) and ANU³⁰ (dashed blue) ice histories. Black markers with 2σ error
371 bars show two-way (circles) or lower-bound (triangle) relative sea-level constraints from
372 ref. ⁹.
373

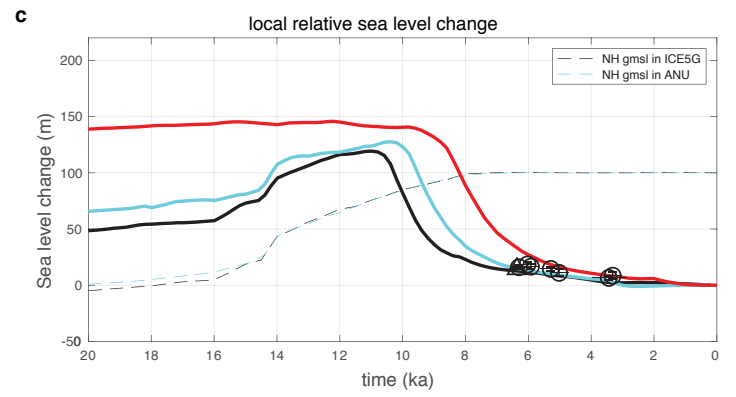
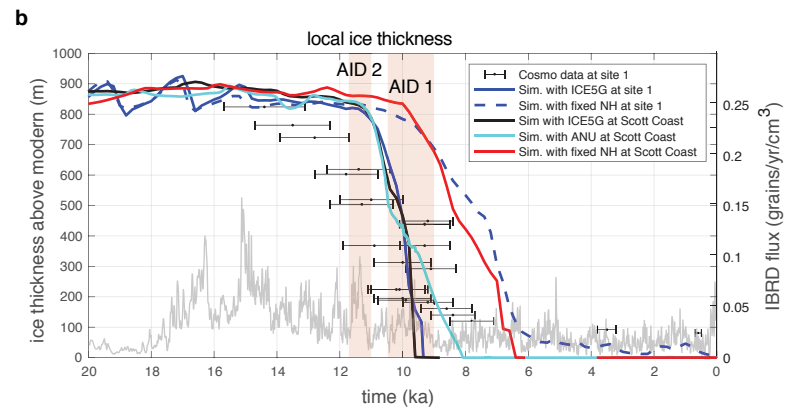
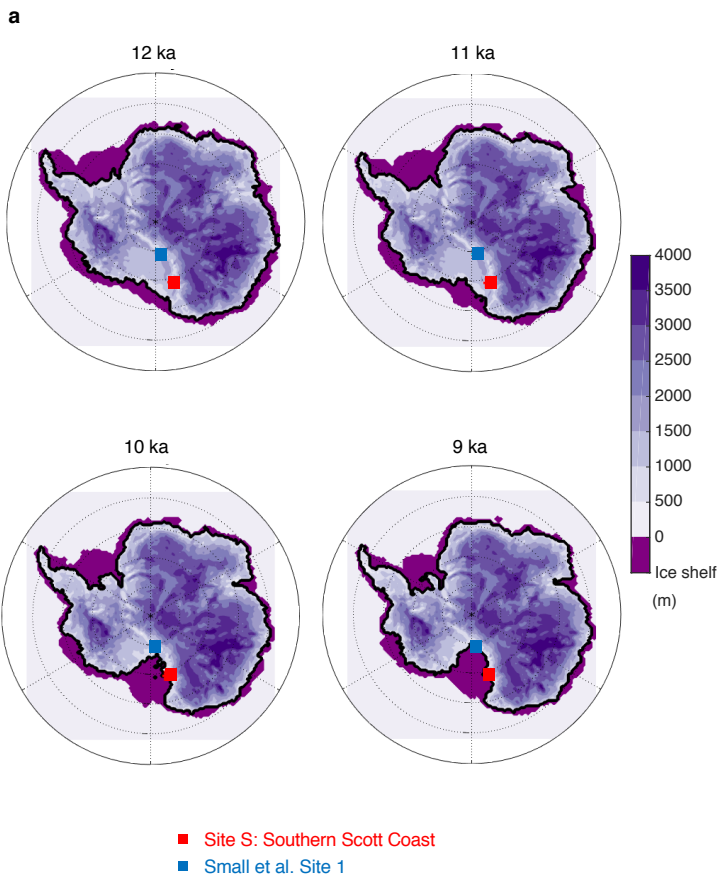
374

375









376 **Methods:**

377 **Coupled ice sheet - sea level modeling**

378 The evolution of the AIS and global sea-level changes was modeled using the
379 coupled ice sheet – sea level model developed and described in detail in ref. ²⁶ and
380 applied in refs. ³⁶ and ²⁸. The model consists of the PSU 3-D ice-sheet model³⁷ coupled to
381 a gravitationally self-consistent global sea-level model that includes viscoelastic
382 deformation of the solid Earth, rotational feedbacks onto sea level and migrating
383 shorelines^{38,39}.

384 PSU 3-D is a finite difference, ice sheet – ice shelf model that adopts hybrid
385 combinations of the scaled Shallow-Ice and Shallow-Shelf equations^{40,41} to treat ice
386 dynamics, and includes grounding-line migration through a parameterization of flux
387 across the grounding line¹⁷. This grounding line treatment performs reasonably well in
388 comparison with higher order ice-sheet models⁴² and facilitates the computational
389 feasibility of glacial-interglacial timescale simulations. Basal sliding in the model is
390 treated with a standard Weertman-type sliding law and basal sliding coefficients are
391 determined through inverse fitting to ice thickness under regions with grounded ice in the
392 modern⁴³. In modern oceanic regions, where basal sliding is relatively unconstrained, the
393 coefficient is set to $10^{-5} \text{ m a}^{-1} \text{ Pa}^{-2}$ in simulations presented in the main text and to 10^{-6} m
394 $\text{a}^{-1} \text{ Pa}^{-2}$ in additional simulations summarized in Extended Data Fig. 1, representing the
395 range identified in ref. ²⁸ to best fit a suite of paleo ice-sheet and sea-level constraints.
396 Note that alternate basal sliding laws have been proposed^{44,45} but model treatments
397 remain unverified by observations and should be explored further in future work. Other
398 ice model parameters such as the calving coefficient and ocean melt factor are similarly

399 set to the best fitting values identified in refs. ¹⁴ and ²⁸. Here and in these references,
400 atmospheric climate forcing was applied by perturbing modern climatology (ALBMAP⁴⁶)
401 to mimic past conditions according to a deep-sea $\delta^{18}\text{O}$ stack⁴⁷. Sub-ice shelf melt rates
402 are determined through a parameterization that depends on subsurface oceanic
403 temperatures from ref. ⁴⁸ with sensitivity inferred from the aforementioned large
404 ensemble model-data comparisons²⁸. We note that the best fitting simulations in these
405 studies produce a relatively small contribution from the Antarctic to sea level over the
406 last deglaciation. We therefore explore simulations with a larger excess ice volume at the
407 Last Glacial Maximum and greater ice loss through the deglaciation in Extended Data
408 Fig. 1.

409 NH ice-cover variations were prescribed in the global sea-level model using five
410 different ice histories: Three global ice histories, ICE5G²⁷, ICE6GC³¹ and the ANU
411 model³⁰, and two histories with GLAC1D reconstructions²⁹ over North America and
412 Greenland, and ICE5G elsewhere. These ice history reconstructions are widely used,
413 cover the whole time period under consideration and are constrained by glacial isostatic
414 adjustment modeling and a suite of sea-level and ice-cover records.

415 Elastic and density structure of the solid Earth in the sea-level model is prescribed
416 from the Preliminary Reference Earth Model (PREM)⁴⁹. Two different models of the
417 viscosity structure of the Earth's mantle are adopted in the simulations. Figures in the
418 main text show results using the 'LVZ' model representative of structure beneath the
419 West Antarctic. The model is characterized by a 50-km thick lithosphere, a low viscosity
420 zone of 10^{19} Pa s extending from the base of the lithosphere to 200 km depth, and a
421 viscosity set to 2×10^{20} Pa s and 3×10^{21} Pa s in the remaining the upper mantle and in the

422 lower mantle, respectively. The LVZ model was adopted in refs. ²⁸ and ³⁶ Additional
423 simulations in Extended Data Fig. 1 adopt a viscosity structure that falls within a range of
424 models that best fit a suite of observations related to glacial isostatic adjustment^{30,50}. The
425 model, labeled ‘HV’, has a lithospheric thickness of 120 km and upper and lower mantle
426 viscosities of 5×10^{20} and 5×10^{21} Pa s, respectively.

427 The ice-sheet model is run on a polar stereographic projection with a 20-km grid
428 resolution, while sea-level calculations are performed up to spherical harmonic degree
429 512. To couple the models, the ice-sheet model first computes changes in Antarctic ice
430 thickness over a 200 year ‘coupling interval’ (sensitivity tests described in ref. ²⁶ show
431 that this choice is sufficiently short for ice-age simulations). These AIS changes are then
432 combined with NH ice cover (which is either fixed at its configuration at 40 ka
433 throughout the run for “fixed NH ice” simulations, or evolves according to the chosen ice
434 history in “evolving NH ice” simulations; See also Extended Data Fig. 8) over this
435 interval, and the combination is used as input to the sea-level model to compute the
436 associated global changes in sea level. The predicted sea-level changes, which are
437 equivalent to the negative of topography or bedrock elevation changes, are passed back to
438 the ice-sheet model and used to update bedrock topography in Antarctica. The ice-sheet
439 model then proceeds forward across another coupling interval and the process repeats
440 over the full 40-kyr simulation. Initial conditions of the ice sheet at 40 ka are provided by
441 a longer, full glacial cycle run of the ice-sheet model along with bedrock deformation
442 given by a simpler Elastic Lithosphere Relaxed Asthenosphere (ELRA) model⁵¹. Global
443 topography and bedrock elevation in Antarctica at the start of the simulation at 40 ka are
444 initially unknown and determined through an iterative procedure in which the predicted

445 modern topography at the end of a 40 ka simulation is compared to observed topography
446 (ETOPO2, ref. ⁵² globally and Bedmap2, ref. ³²) in Antarctica and the difference between
447 the two is used to correct the initial topography at 40 ka in the next iteration. The process
448 is repeated four times, which guarantees sufficient convergence of predicted and
449 observed modern topography.

450

451 **Iceberg Alley sites and IBRD record**

452 Sample-based investigations concentrated on deep-sea cores retrieved in the Scotia
453 Sea's Iceberg Alley during Marion Dufresne II cruise 160 in March 2007. Sites MD07-
454 3133 (57°26'S, 43°27'W; 3101 m water depth; 32.8 m long) and MD07-3134 (59°25'S,
455 41°28'W; 3663 m water depth; 58.2 m long) originate from the northern end of Dove
456 Basin and Pirie Bank, respectively.

457 The age models of sites MD07-3133 and MD07-3134 are based on distinct dust-
458 climate couplings between Southern Ocean sediment and the Antarctic EPICA Dronning
459 Maud Land (EDML) ice core⁵³ on the EDML1 age model⁵⁴, which appears more
460 consistent with local ash layer correlations than the later AICC 20102 age model^{55,56},
461 which relies on interhemispheric methane correlation. Comparison between age models
462 (Extended Data Fig. 9c) shows older ages for the AICC 2012 age scale. Differences are
463 minimal for the mid to late Holocene. At the time of MWP-1B the difference is on the
464 order of 150 years, whereas it is 350 years during MWP-1A and ~500 years at LGM.
465 This means that for AID event 2 the shift is very small and the event aligns well with
466 MWP-1B regardless of the age model. AID event 6 would extend from ~14.3–15.2 ka in
467 AICC 2012, a range that still encompasses MWP-1A (14.65-14.3 ka), especially within

468 the uncertainties of the ice-core age models, which increase from a few centuries for the
469 time of MWP-1B up to millennium for the last glacial maximum^{55,56}. Therefore, the
470 correlations we make here and the conclusions we draw hold regardless of the age model
471 applied.

472 The use of magnetic susceptibility as well as Ca and Fe records measured through
473 X-ray fluorescence is considered a well-established approach to study coherent and
474 synchronous changes in dust deposition across much of the Southern Ocean and the AIS
475 across the last deglaciation⁴ as well as on longer, glacial-to-interglacial times scales^{57,58}.

476 IBRD counting was conducted every centimeter on x-radiographs taken from 1-cm
477 thick slices that were cut out from the center of each core segment and exposed to an x-
478 ray system. The transitions from low to high and high to low IBRD contents form the
479 basis of our AID event classification. The counting interval of 1 cm translates into 8–17
480 years resolution for AID 1–7, depending on the time interval and core. The IBRD data is
481 presented here is a stack of Sites MD07-3133 and MD07-3134 to obtain a regional rather
482 than a local record for the time 20–0 ka. It is combined from previous publications for the
483 period 27–7 ka⁴ and 8–0 ka²⁴. This new IBRD stack with the EDML1 and AICC 2012
484 age models along with uncertainty calculations are shown in Extended Data Fig. 9c and
485 three tables containing the IBRD data on both age scales, the age-scale tie points, and the
486 uncertainty calculations can be downloaded from the PANGAEA data server (see link in
487 Data Availability).

488

489 **Comparison to Cosmogenic Exposure Age Data**

490 In Fig. 4 and Extended Data Figs. 10-11, we compare modeled ice loss history in the
491 Ross and Weddell Sea regions to records of ice thinning from cosmogenic exposure age
492 data from ref. ³⁵, also discussed in ref. ⁵⁹. Records at Site 1 in the Ross Sea (Fig. 4) and at
493 Sites 11-15 in the Weddell Sea region (Extended Data Fig. 10 are consistent with the
494 earlier deglaciation predicted in simulations that include a NH sea-level forcing. While
495 exposure age data at Sites 3-5 (Extended Data Fig. 11a) appear to be more consistent with
496 a later deglaciation, these sites are just outside of the region of significant ice loss in the
497 simulation (Extended Data Fig. 11d, e). The sites are geographically close to Site S, but
498 they exhibit substantially less thinning than the rest of the Ross Sea region (compare ice
499 loss at red and blue stars in Extended Data Fig. 11e). Thinning rates and timing at Sites 1
500 and S, on the other hand, are comparable (Extended Data Fig. 11 and Fig. 4b of the main
501 text) and more representative of regional-scale ice loss that occurs in the model during
502 the main part of the deglaciation. Taken into consideration with the Ross Sea grounding
503 line record⁷, it is possible that major deglaciation ends in this sector of the Ross Sea by
504 around 8 ka and the thinning rates observed at Sites 3-5 indicate smaller magnitude, late
505 Holocene ice changes. Higher resolution ice sheet modeling would be needed to
506 investigate this issue further, which is infeasible in the long timescale coupled models
507 described in the current study.

508

509 **Data Availability**

510 The datasets generated in this publication are available both within the PANGAEA data
511 base system (<https://doi.pangaea.de/10.1594/PANGAEA.919498>)
512 (doi:10.1594/PANGAEA.919498) and as source data for Extended Data Figure 9. The

513 modeling results are available at the following OSF database:

514 https://osf.io/g5ur2/?view_only=8acbf1e38c184d9c8f09811c8bbef036

515

516 **Code Availability**

517 The coupled ice sheet – sea level model used in this manuscript has been reported in

518 refs.²⁶ and ²⁸, with the PSU-3D ice sheet model reported in the following reference:

519 <https://doi.org/10.5194/gmd-5-1273-2012>. The ice model is available upon request from

520 the developer, David Pollard, and the sea level model is available from Jerry Mitrovica.

521

522 **Acknowledgements**

523 The contributions of N.G. and H.K.H. were supported by the Natural Sciences and

524 Engineering Research Council (NSERC), the Canada Research Chair’s program and the

525 Canadian Foundation for Innovation, M.E.W. by the Deutsche Forschungsgemeinschaft

526 (DFG grant numbers We2039/8-1 and We 2039/17-1), and J.X.M. by NASA grant

527 NNX17AE17G and Harvard University. We thank Gabriel Tseng for assistance with

528 exploratory research that informed this study, and David Pollard for insight on and use of

529 the PSU ice sheet model.

530

531 **Author Contributions**

532 N.G. contributed the numerical modeling and analysis, H.K.H. prepared model input,

533 M.E.W contributed IBRD records and together with P.U.C. and J.X.M. other published

534 data and related discussion, and all authors contributed to developing the idea and writing

535 and refining the manuscript.

536

537 **Author Information**

538 Correspondence should be addressed to Natalya Gomez (natalya.gomez@mcgill.ca).

539 Reprints and permissions information is available at www.nature.com/reprints.

540

541 **Competing interests**

542 The authors declare no competing interests.

543

544 **References for Methods:**

545

- 546 36 Gomez, N., Pollard, D. & Holland, D. Sea-level feedback lowers projections of
547 future Antarctic Ice-Sheet mass loss. *Nature Communications* **6**, 8798,
548 doi:10.1038/ncomms9798 (2015).
- 549 37 Pollard, D. & DeConto, R. M. Description of a hybrid ice sheet-shelf model, and
550 application to Antarctica. *Geoscientific Model Development Discussions* **5**,
551 1077-1134, doi:10.5194/gmdd-5-1077-2012 (2012).
- 552 38 Kendall, R. A., Mitrovica, J. X. & Milne, G. A. On post-glacial sea level - II.
553 Numerical formulation and comparative results on spherically symmetric
554 models. *Geophysical Journal International* **161**, 679-706 (2005).
- 555 39 Gomez, N., Mitrovica, J. X., Tamisiea, M. E. & Clark, P. U. A new projection of
556 sea level change in response to collapse of marine sectors of the Antarctic Ice
557 Sheet. *Geophysical Journal International* **180**, 623-634, doi:10.1111/j.1365-
558 246X.2009.04419.x (2010).
- 559 40 MacAyeal, D. R. Large-scale ice flow over a viscous basal sediment: Theory
560 and application to ice stream B, Antarctica. *Journal of Geophysical Research:
561 Solid Earth* **94**, 4071-4087, doi:10.1029/JB094iB04p04071 (1989).
- 562 41 Hutter, K. Theoretical glaciology: material science of ice and the mechanics of
563 glaciers and ice sheets, Reidel Publ. Co., Dordrecht (1983).
- 564 42 Pattyn, F. *et al.* Grounding-line migration in plan-view marine ice-sheet
565 models: results of the ice2sea MISIP3d intercomparison. *Journal of
566 Glaciology* **59**, 410-422, doi:10.3189/2013JoG12J129 (2013).
- 567 43 Pollard, D. & DeConto, R. M. A simple inverse method for the distribution of
568 basal sliding coefficients under ice sheets, applied to Antarctica. *The
569 Cryosphere* **6**, 953-971, doi:10.5194/tc-6-953-2012 (2012).
- 570 44 Pattyn, F. Sea-level response to melting of Antarctic ice shelves on multi-
571 centennial time scales with the fast Elementary Thermomechanical Ice Sheet
572 model (f.ETISh v1.0). *The Cryosphere Discussions*, 1-52, doi:10.5194/tc-2017-
573 8 (2017).

574 45 Tsai, V. C., Stewart, A. L. & Thompson, A. F. Marine ice-sheet profiles and
575 stability under Coulomb basal conditions. *Journal of Glaciology* **61**, 205-215
576 (2015).

577 46 Le Brocq, A. M., Payne, A. J. & Vieli, A. An improved Antarctic dataset for high
578 resolution numerical ice sheet models (ALBMAP v1). *Earth System Science*
579 *Data Discussions* **3**, 195-230, doi:10.5194/essdd-3-195-2010 (2010).

580 47 Lisiecki, L. E. & Raymo, M. E. A Pliocene-Pleistocene stack of 57 globally
581 distributed benthic $\delta^{18}O$ records. *Paleoceanography* **20**,
582 doi:10.1029/2004PA001071 (2005).

583 48 Liu, Z. *et al.* Transient simulation of last deglaciation with a new mechanism
584 for Bolling-Allerod warming. *Science* **325**, 310-314,
585 doi:10.1126/science.1171041 (2009).

586 49 Dziewonski, A. M. & Anderson, D. L. Preliminary reference Earth model
587 (PREM). *Physics of the Earth and Planetary Interiors*, 1-60 (2011).

588 50 Mitrovica, J. X. & Forte, A. M. A new inference of mantle viscosity based upon
589 joint inversion of convection and glacial isostatic adjustment data. *Earth and*
590 *Planetary Science Letters* **225**, 177-189 (2004).

591 51 Huybrechts, P. & de Wolde, J. The dynamic response of the Greenland and
592 Antarctic ice sheets to multiple-century climatic warming. *Journal of Climate*
593 **12**, 2169-2188 (1999).

594 52 National Geophysical Data Center, NOAA. *2-minute Gridded Global Relief Data*
595 *(ETOPO2) v2.* , 2006).

596 53 Weber, M. E. *et al.* Dust transport from Patagonia to Antarctica - A new
597 stratigraphic approach from the Scotia Sea and its implications for the last
598 glacial cycle. *Quaternary Science Reviews* **36**, 177-188,
599 doi:10.1016/j.quascirev.2012.01.016 (2012).

600 54 Ruth, U. *et al.* "EDML1": a chronology for the EPICA deep ice core from
601 Dronning Maud Land, Antarctica, over the last 150 000 years. *Climate of the*
602 *Past* **3**, 475-484 (2007).

603 55 Veres, D. *et al.* The Antarctic ice core chronology (AICC2012): an optimized
604 multi-parameter and multi-site dating approach for the last 120 thousand
605 years. *Clim. Past* **9**, 1733-1748, doi:10.5194/cp-9-1733-2013 (2013).

606 56 Bazin, L. *et al.* An optimized multi-proxy, multi-site Antarctic ice and gas
607 orbital chronology (AICC2012): 120–800 ka. *Clim. Past* **9**, 1715-1731,
608 doi:10.5194/cp-9-1715-2013 (2013).

609 57 Lamy, F. *et al.* Increased dust deposition in the Pacific Southern Ocean during
610 glacial periods. *Science* **343**, 403-407, doi:10.1126/science.1245424 (2014).

611 58 Martínez-García, A. *et al.* Iron Fertilization of the Subantarctic Ocean During
612 the Last Ice Age. *Science* **343**, 1347-1350, doi:10.1126/science.1246848
613 (2014).

614 59 Small, D., Bentley, M. J., Jones, R. S., Pittard, M. L. & Whitehouse, P. L. Antarctic
615 ice sheet palaeo-thinning rates from vertical transects of cosmogenic
616 exposure ages. *Quaternary Science Reviews* **206**, 65-80 (2019).

617

618

619 **EXTENDED DATA FIGURE CAPTIONS**

620 **Extended Data Figure 1: Sensitivity of results to ice and Earth model parameters.**
621 (a) Changes in Antarctic ice volume predicted in simulations with evolving (solid lines)
622 and fixed (dashed lines) NH ice mass and the LVZ (“low viscosity zone”) Earth model
623 (see Methods). Blue lines are identical to those in Fig. 2b of the main text, adopting a
624 basal sliding coefficient of $10^5 \text{ m a}^{-1} \text{ Pa}^{-2}$, while red lines adopt a basal sliding coefficient
625 for a stickier marine bed of $10^6 \text{ m a}^{-1} \text{ Pa}^{-2}$. (b) As in (a) but adopting the HV (“high
626 viscosity”) Earth model (see Methods). Black dotted lines and right-hand-side y-axis in
627 each frame show changes in NH ice volume, in meters of global mean sea level
628 equivalent (GMSLE), prescribed in the ICE5G²⁷ ice history. For reference, blue and red
629 vertical bands in (a) and (b) represent the timing of MWP and AID events as described in
630 Figure 2a and 2c of the main text, respectively.

631
632 **Extended Data Figure 2: Evolution of Antarctic ice cover with and without NH sea-**
633 **level forcing.** Columns: Thickness of grounded ice in meters and extent of ice shelves at
634 30 ka, 20 ka, 10 ka and the modern as labeled, predicted from simulations that include
635 variations in the NH ice sheets represented by the ICE5G²⁷ ice history (row a) and
636 simulations in which ice cover in the NH remains fixed (row b). Black lines in rows (a)
637 and (b) show the grounding lines. Row c shows the difference in grounded ice thickness
638 between simulations in rows (a) and (b), representing the impact of sea-level changes
639 associated with NH ice sheets on the evolution of the AIS. Green and black lines
640 represent the positions of the grounding lines with (row a) and without (row b) the NH
641 sea-level forcing included.

642
643 **Extended Data Figure 3: Influence of NH sea-level forcing on Antarctic ice cover**
644 **during the deglaciation.** Differences in thickness of grounded ice at the indicated times,
645 in meters, between simulations that include variations in the NH ice sheets from ICE5G²⁷
646 ice history and in which ice cover in the NH remains fixed throughout the simulation.
647 Differences are displayed as in Fig. 3c of the main text, but every 1 ky for the last 20 ka.
648 Green and black lines represent the positions of the grounding lines with and without the
649 NH sea-level forcing included, respectively.

650
651
652 **Extended Data Figure 4: Antarctic ice volume changes in the Ross and Weddell Sea**
653 **sectors.** (a) Changes in ice volume in the Ross Sea sector predicted in simulations with
654 fixed (red line) and evolving (black line) NH ice from the ICE5G ice history. (b) As in
655 frame (a) but for the Weddell Sea sector. (c) Blue lines outline the areas included in the
656 calculations in frames (a) and (b), and background colors indicate the change in ice
657 thickness in meters from 20 ka to the modern in the simulations that includes NH ice
658 cover changes from ICE5G²⁷.

659
660 **Extended Data Figure 5: Influence of NH sea-level forcing on rate of Antarctic ice**
661 **loss.** (a-e) Rate of change of Antarctic ice volume, including grounded and floating ice,
662 calculated with a 100 year running mean, predicted from simulations including (black
663 lines) and excluding (red lines) NH ice-cover changes, using the ice histories indicated in

664 the legend (see Methods). Note that Fig. 3a of the main text shows the mean and standard
665 deviation of these five frames.

666

667 **Extended Data Figure 6: Patterns of sea-level change for Antarctic ice loss during**
668 **MWP-1A and the early Holocene.** (a-b) Predicted sea-level change, normalized by the
669 global mean sea-level equivalent (GMSLE) associated with Antarctic ice loss during (a)
670 MWP-1A and (b) the early Holocene including MWP-1B. Calculations are associated
671 with simulations that include a NH forcing given by ICE5G²⁷. The patterns of sea-level
672 change and the GMSLE used in the normalization are calculated over the time windows
673 given by the grey bands in Fig. 3a of the main text. Green and magenta stars indicate
674 locations of far-field relative sea-level records in Tahiti and Barbados.

675

676 **Extended Data Figure 7: Sensitivity of the Weddell Sea sector to geographic**
677 **variability in sea-level forcing.** (a) Change in ice thickness predicted from a simulation
678 adopting the ICE5G²⁷ ice history in the NH that includes geographically variably sea-
679 level changes associated with gravitational, deformational and Earth rotational effects
680 activated by ice-cover changes globally during MWP-1A from 14.5-13.5 ka. Grey and
681 black lines in (a) indicate the grounding-line position at the start and end of the time
682 interval, respectively. This frame is the same as Fig. 3b of the main text but zoomed in on
683 the Weddell Sea region where geographically variable sea-level changes associated with
684 NH ice loss are largest (see Fig. 1c). (b) The difference between (a) and the same
685 calculation adopting the simulation with globally uniform sea-level change from the NH.
686 The black line in (b) is as in frame (a) and the blue lines indicates the grounding-line
687 position at the end of the time interval for the uniform sea-level simulation. (c) Antarctic
688 ice volume variations from simulations with geographically variable (black line) and
689 uniform (red line) sea-level changes associated with NH ice loss over the MWP-1A
690 interval. Frames (d-f) are as in (a-c) but for the early Holocene interval from 11.5-9 ka. In
691 this case, frame (d) is as in Fig. 3d of the main text but zoomed in on the Weddell Sea
692 region. Note that the uniform sea-level change is calculated relative to modern
693 topography, and scaled such that the total contribution to eustatic sea-level change from
694 the NH over the last deglaciation from 21 ka on is 95.5 meters, in agreement with ref. ²⁷.

695

696 **Extended Data Figure 8: Predicted Antarctic ice volume changes and GMSLE**
697 **contributions.** (a) Changes in AIS volume predicted in a simulation with NH ice cover
698 fixed at the 40 ka configuration within ICE5G²⁷ (solid red line), and in simulations with
699 evolving NH ice adopting the ICE5G²⁷ (solid black line), ICE6GC³¹ (dashed black line)
700 and the ANU³⁰ model (cyan line) ice histories, as well as two composite ice histories in
701 which ice cover over North America and Greenland in ICE5G has been replaced by
702 regional GLAC1D²⁹ models (blue lines). Finally, the dashed red line represents a
703 simulation in which the NH ice sheets are fixed at the modern configuration rather than at
704 the 40 ka configuration throughout the simulation. In this case, marine-based sectors of
705 the AIS start on even shallower bedrock, and hence the predicted ice sheet growth is
706 larger at the Last Glacial Maximum, while the ice loss during the deglaciation occurs
707 later and is of even smaller magnitude than in the original simulation. Note that this is not
708 a realistic starting configuration. Frame (b) is as in frame (a) but expressed as a GMSL
709 equivalent relative to the modern state. This is calculated by taking the ice above

710 floatation thickness in Antarctica relative to the paleo bedrock topography at each time
711 step in the model, and dividing by the area of the modern ocean. Note that frames (a) and
712 (b) are not directly proportional because as the bedrock topography in Antarctica evolves
713 the volume of ice above floatation in marine sectors also changes. Blue and red vertical
714 bands in (a) and (b) represent the timing of MWP and AID events as described in Figure
715 2a and 2c of the main text, respectively.

716

717 **Extended Data Figure 9: Age model comparison and uncertainty for IBRD flux**
718 **record from Iceberg Alley.** (a) Age difference between the AICC 20102 age model^{55,56}
719 and EDML1 age model⁵⁴. (b) Age uncertainty in the AICC 2012 age model. (c) IBRD
720 flux time series adopting the AICC 2012 (black line, as in Figs. 2c and 4b of the main
721 text) and EDML 1/EDC 3 (blue line) age scales. The IBRD stack is composed of records
722 from Sites MD07-3133 and MD07-3134. It is presented here for the time 20–0 ka and
723 was combined from previous publications for the period 27–7 ka⁴ and 8–0 ka²⁴. Vertical
724 brown bars indicate AID 1-7⁴ on the AICC 2012 age scale. Blueish vertical bars indicate
725 the times of MWP-1A²¹ and MWP-1B²². Horizontal black error bars at the top of frame
726 (c) show propagated uncertainties for the upper and lower bounds of each AID event for
727 errors in tie point correlation to EDML⁴ and uncertainties of the AICC 2012 age model.

728

729 **Extended Data Figure 10: Comparison of predicted and observed ice thickness**
730 **changes in the Weddell Sea region.** (a-b) Predicted (lines) and observed (error bars) ice
731 thickness above modern thickness in meters at (a) Sites 11-13 and (b) Sites 14-15 from
732 ref. ³⁵. (c) Map of predicted ice thickness at 12 ka in the simulation with ICE5G²⁷ with
733 locations of the sites discussed in the Weddell Sea and Ross Sea (see Extended Data
734 Figure 10) as indicated. Predictions are from simulations in which NH ice cover is
735 evolving according to ICE5G²⁷ (black lines) and fixed (blue lines), respectively. Error
736 bars show cosmogenic exposure age data with 2σ uncertainty from ref. ³⁵. See Methods
737 section for further discussion of these results.

738

739 **Extended Data Figure 11: Comparison of predicted and observed ice thickness**
740 **changes in the Ross Sea region.** (a) Predicted (lines) and observed (2σ error bars) ice
741 thickness above modern thickness in meters at Scott Coast Site S discussed in the main
742 text and at Sites 1 (red) and 3-5 (shades of blue) from ref. ³⁵. Locations of the sites are
743 indicated on the maps in frames b-e. Predictions are from simulations in which NH ice
744 cover is evolving according to ICE5G²⁷ (solid lines) and fixed (dashed lines),
745 respectively. Observations are cosmogenic exposure age data from ref. ³⁵. Red vertical
746 bands represent the timing of AID events 1 and 2 as described in Fig. 2c of the main text.
747 (b) Map of predicted ice thickness at 12 ka in the Ross Sea in the simulation with
748 ICE5G²⁷. (c-e) The difference in ice thickness between 12 ka (frame b) and 11, 10, and 9
749 ka, respectively. See Methods for further discussion of these results.

750